

Comparison between the First Order Statistical Analysis and Higher Order Statistical Analysis on Characterization of Brain Tumor on CT Images

Auis Bashir¹, Mohammed Garelnabi¹, Shazaly Khojaly^{1,2}, Magdi Hassan² Shaza Elfadil¹

¹ Sudan University for Sciences and Technology, College of Radiological Sciences, Khartoum, Sudan
Khartoum east, Khartoum, Sudan

² Hamad Medical Corporation, Clinical Imaging Department, Ultrasound Section, Doha , Qatar

Abstract: This study had been worked up on hundred and nine CT images of different types of brain tumor. For the first order statistical analysis the procedure contain dual phase, phase one contain textural feature extraction from the selected images (features included: mean, skewness, energy and entropy), phase two classification of images component according to their extracted textural features using linear discriminant analysis, the results showed that the proposed method have achieved high accuracy in recognizing the intracranial tumor from the normal surrounding tissues. The accuracy of classification was 90.4%. For the higher order statistical analysis nine features include; long run emphasis, low gray-level run emphasis , high gray-Level, Run emphasis, short run low gray-level emphasis , short run high gray-Level emphasis, long run low gray-level emphasis, long run high gray-level emphasis, gray-level non-uniformity, run length non-uniformity, run percentage had been used for image classification. The analyzed data showed accuracy percentage beyond to 94%. That exploring the priority of higher order statistical analysis method upon the first order on classification of brain tumor when the classification process based on the tumor textural feature.

Keywords: classification, texture feature, first order, second order statistical analysi, computed tomography CT, brain tumor

1. Introduction

Texture analysis has been used to identify unique pathology on multi-modality images of cancer patients. Using the local binary operator to analyse the weak underlying textures found in transrectal ultrasound images of the prostate, Kachouie and Fieguth demonstrated that the approach was suitable for segmentation of the prostate (Kachouie & Fieguth, 2007). In another cancer-related study of 48 normal images and 58 cancer images of the colon, Esgiar et al., demonstrated that by adding a fractal feature to traditional statistical features the sensitivity of the classification improved (Esgiar et al., 2002).

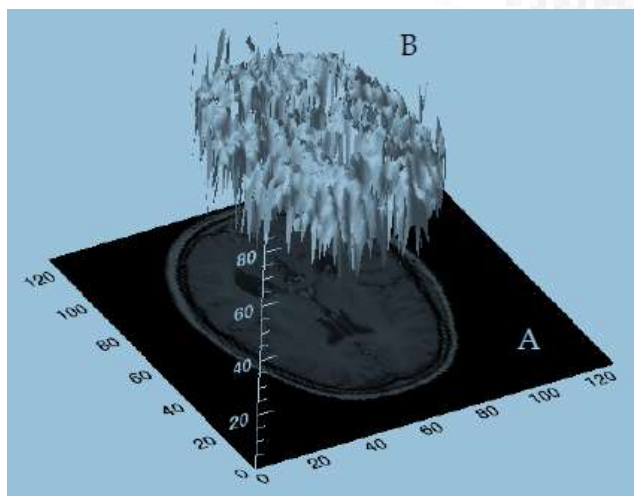


Figure (2-8): Three dimensional textured intensity surface representation of a medical image. A: Two-dimensional MR image of the brain. B: Pixel values of the MR image plotted

on the vertical axis to produce a 3D textured surface (William Henry Nailon (2010)

2. About CT

Computed tomography involves passage of a collimated X - ray beam through the patient to obtain images of thin transverse sections of the head and body. A sensitive detection system with photomultiplier tubes is employed, with the X - ray tube rotating around the patient during each cycle. An image is obtained by computer processing of the digital readings from the photomultiplier tubes and analysis of the absorption pattern of each tissue. Absorption values are expressed on a scale of +1,000 units for bone, the maximum absorption of the X - ray beam, to - 1,000 units for air, the least absorbent. (Pradip R. Patel 2010)

In other words it is an ideal form of tomography yielding sequence images of thin consecutive slices of the patient and providing the opportunity to localise in three dimensions. Unlike conventional, classical tomography, computerised tomography does not suffer from interference from structures in the patient outside the slice being imaged. This is achieved by irradiating only thin slices of the patient with a fan-shaped beam. Transaxial images (tomograms) of the patient's anatomy can give more selective information than conventional planar projection radiographs. Compared to planar radiography, CT images have superior contrast resolution, (Mikael Sandborg, 1995)

Projection data are a result of interaction between the radiation used for imaging and the substance of which the object is composed. For x-ray tomography, the measured photon energy of an x-ray beam reduces while going through

Volume 7 Issue 8, August 2018

www.ijsr.net

Licensed Under Creative Commons Attribution CC BY

an object. The mechanisms mainly causing this are the photoelectric effect (absorption) and the Compton effect (scattering). The photon loss rates of a narrow mono-energetic x-ray beam while going through a material is an indication for the linear attenuation coefficient of that material

$$N(x) = N_0 e^{-\mu x}$$

In practice x-ray sources do not produce mono-energetic beams. Filtering of the x-ray beam to get photons in a narrow energy-band would greatly reduce the number of photons available and is therefore not advisable. The linear attenuation coefficient is, in general a function of the photon energy. For most biological tissues, the linear attenuation coefficient decreases with energy. Low energy photons are preferentially absorbed in those tissues resulting in beam hardening, which may cause artifacts. (Marjolein van der Glas, 2000)

To reconstruct an object from a projection made with a polychromatic x-ray, it is necessary to know the effective energy of the CT scanner. This is defined as the monochromatic energy at which a given material will exhibit the same attenuation as measured by the scanner. The output of a CT scanner is given in Hounsfield units. Theoretically, the relation between the linear attenuation coefficient (μ) and the corresponding Hounsfield unit (H) is:

$$H = \frac{\mu_{material} - \mu_{water}}{\mu_{water}} * 1000$$

The value of the Hounsfield unit varies from -1000 (for air) to 3000. . (Marjolein van der Glas, 2000)

Table (1-1): Shows the CT numbers in Hounsfield unit for different types of tissues.

Tissue	Range of Hounsfield Units
Air	-1000
Lung	-500 to -200
Fat	-200 to -50
Water	0
Blood	25
Muscle	25 to 40
Bone	200 to 1000

Materials:

CT scanner machines:

Neusoft dual slice and GE 8 slice MDCT scanners

Design of the study:

This is analytic study used CT brain images for intracranial tumor patients for classification texturally and characterization in respect to the tissue appearance on the CT images.

Methodology

Imaging protocols

CT images were done using the following parameters;
 Preparation: not needed unless we used sedation or contrast medium in this case from two to four hours fasting must be

considered, beside RFT test in case of contrast medium using.

Ten day role should be considered for females patients.

Patient position: lying down in supine position

Head first

Head rested on the head holder

No rotation and no tilt of the head are important.

A localizer radiograph is taken prior to the actual CT procedure.

Axial scan started from the base of skull to the vertex.

Slice thickness= 5mm, interval =5mm, matrix size= 512, FOV=250, voltage= 120Kv, current= 150MA, rotation time=1.5second.

3. Statistical Method

a) First order

Mean: Calculates the mean intensity value of all pixels

$$\sigma = \sqrt{\frac{1}{N} \sum_{i=1}^N (x_i - \mu)^2}$$

Skewness: It measures the symmetry of a distribution curve of pixel intensity occurrences as seen in a histogram.

$$\gamma = \frac{\frac{1}{N} \sum_{i=1}^N (x_i - \mu)^3}{\left(\frac{1}{N} \sum_{i=1}^N (x_i - \mu)^2\right)^{\frac{3}{2}}}$$

Energy: $Energy = \sum_i \sum_j (i - j)^2 P_d(i, j)$

Entropy: The entropy of a gray-scale image is a measure of intensity value randomness. It is calculated from the histogram counts of an image giving a probability of certain pixel values occurring in the image.

$$entropy = - \sum_i \sum_j P_d(i, j) \log P_d(i, j)$$

b) Higher order

A gray level run length matrix is defined as: A set of consecutive, collinear pixels having the same gray level, length of the run is the number of pixels in the run.

The run-length matrix p (i, j) is defined by specifying direction 0°, 45°, 90°, 135° and then count the occurrence of runs for each gray levels and length in this direction (i) Dimension corresponds to the gray level (bin values) and has a length equal to the maximum gray level (bin values) n (j) dimension corresponds to the run length and has length equal to the maximum run length (bin values).

The extracted features on higher order statistic were include: long run emphasis, low gray-level run emphasis, high gray-Level, Run emphasis, short run low gray-level emphasis, short run high gray-Level emphasis, long run low gray-level

emphasis, long run high gray-level emphasis, gray-level non-uniformity, run length non-uniformity, run percentage
 Long run emphasis:

$$LRE = \frac{1}{T_R} \sum_{i=0}^{N_g-1} \sum_{j=1}^{N_r} j^2 r'(i, j | \alpha).$$

LRE feature measures distribution of long runs, The LRE is highly depend on the occurrence of long runs and is expected large for coarse structural textures.

Low Gray-Level Run Emphasis:

$$LGRE = \frac{1}{n_r} \sum_{i=1}^M \sum_{j=1}^N \frac{P(i-j)}{i^2}$$

High Gray-Level Run Emphasis:

$$HGRE = \frac{1}{n_r} \sum_{i=1}^M \sum_{j=1}^N P(i-j) - i^2$$

Short Run Low Gray-Level Emphasis

$$SRLGE = \frac{1}{n_r} \sum_{i=1}^M \sum_{j=1}^N \frac{P(i, j)}{i^2 - j^2}$$

Short Run High Gray-Level Emphasis

$$SRHGE = \frac{1}{n_r} \sum_{i=1}^M \sum_{j=1}^N \frac{P(i, j) - i^2}{i^2}$$

Long Run Low Gray-Level Emphasis

$$LRLGE = \frac{1}{n_r} \sum_{i=1}^M \sum_{j=1}^N \frac{P(i-j) - j^2}{i^2}$$

Long Run High Gray-Level Emphasis

$$LRHGE = \frac{1}{n_r} \sum_{i=1}^M \sum_{j=1}^N P(i, j) - i^2 - j^2$$

Gray-Level Non-Uniformity

$$GLN = \frac{1}{n_r} \sum_{i=1}^M \left(\sum_{j=1}^N P(i, j) \right)^2$$

Run Length Non-Uniformity,

$$GLN = \frac{1}{n_r} \sum_{j=1}^N \left(\sum_{i=1}^M P(i, j) \right)^2$$

Run Percentage:

$$RP = \frac{n_r}{n_p}$$

4. Results

First order statistical result

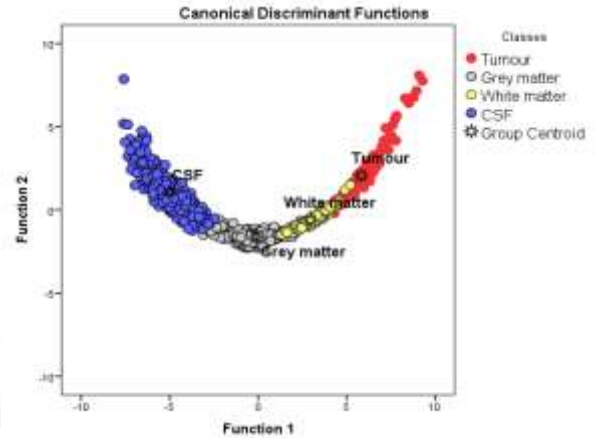


Figure 4.1.1: Scatter pollete shows the classification map

Table 4.1.1 Groups classification accuracy

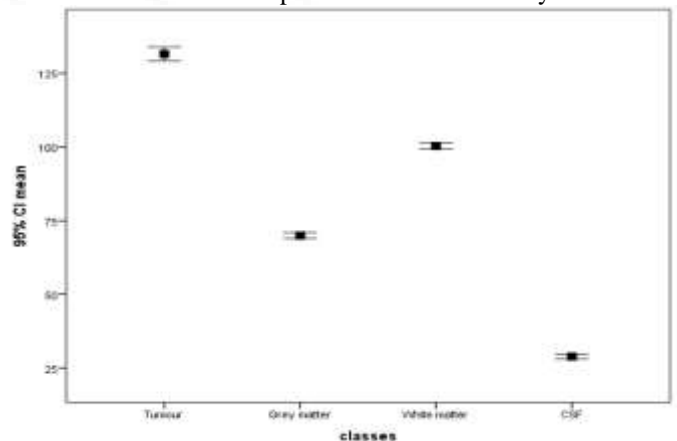


Figure 4.1.2: Error bar shows group classification mean based

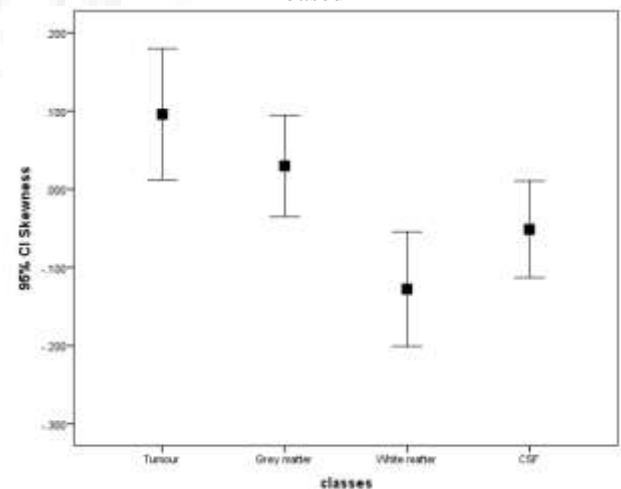


Figure 4.1.3: Error bar shows group classification skewness based

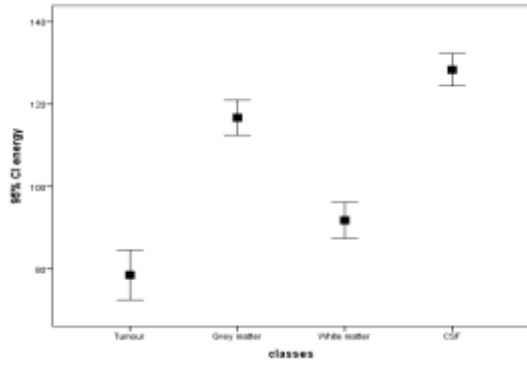


Figure 4.1.4: Error bar shows group classification energy based

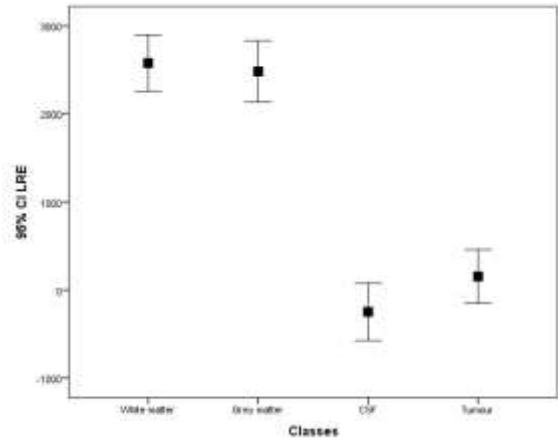


Figure 4.2.2: Error bar shows the classification based on long run emphasis feature

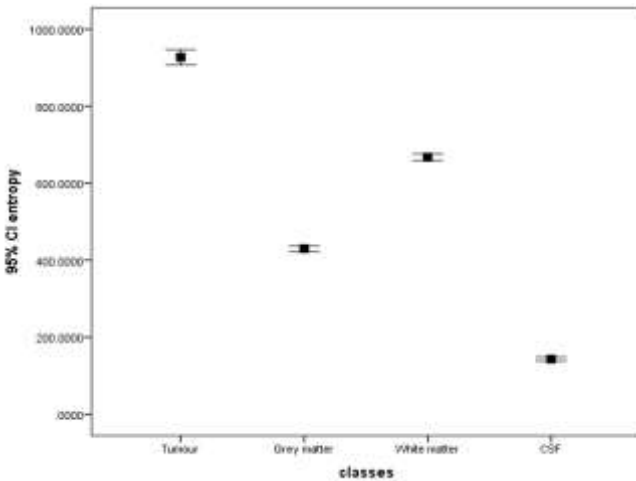


Figure 4.2.5: Error bar shows group classification entropy based

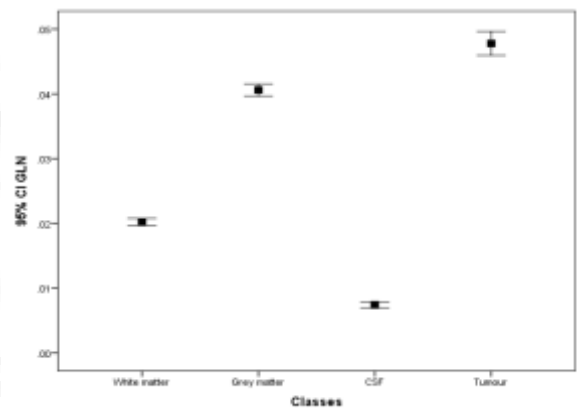


Figure 4.2.3: Error bar shows the classification based on grey level non uniformity feature

4.2 Higher Order Statistic

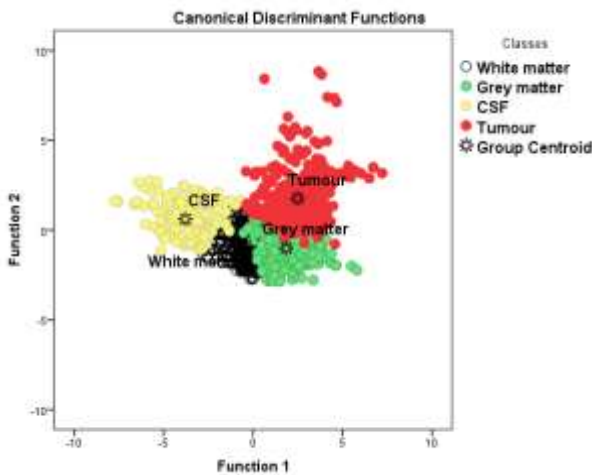


Figure 4.2.1: Scatter graph demonstrates the classification map

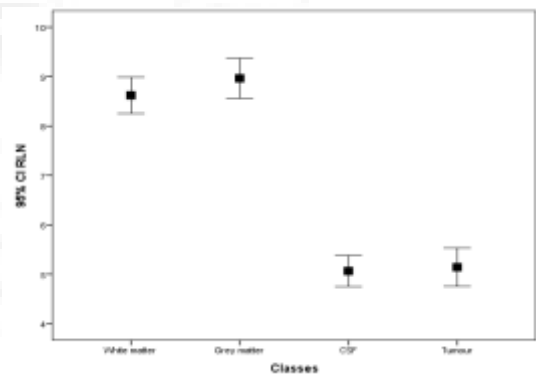


Figure 4.2.4: Error bar shows the classification based on run length non-uniformity feature

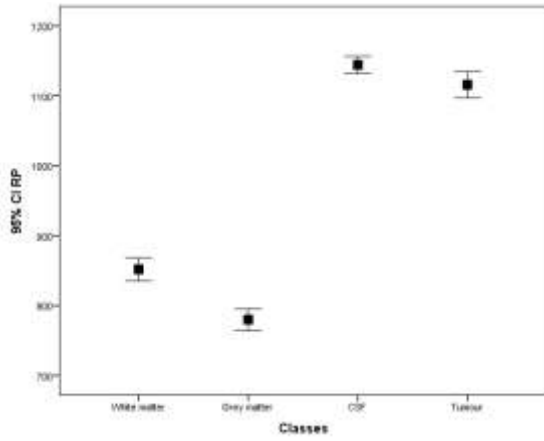


Figure 4.2.5: Error bar shows the classification based on run percentage feature

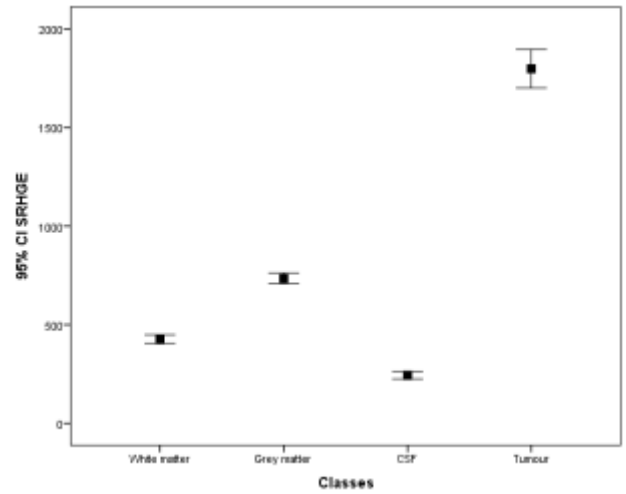


Figure 4.2.8: Error bar shows the classification based on short run high gray-level emphasis feature

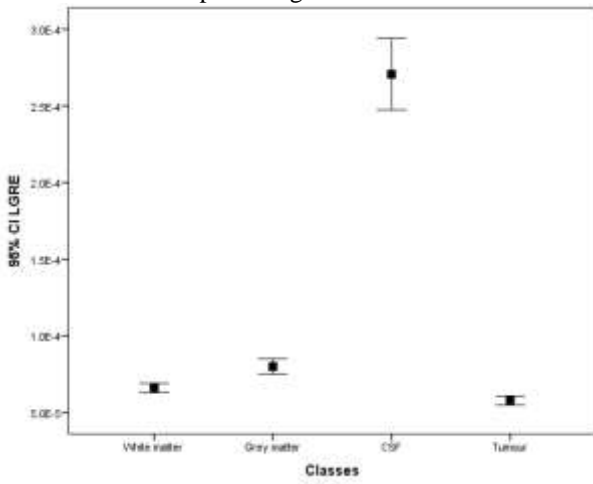


Figure 4.2.6: Error bar shows the classification based on low gray-level run emphasis feature

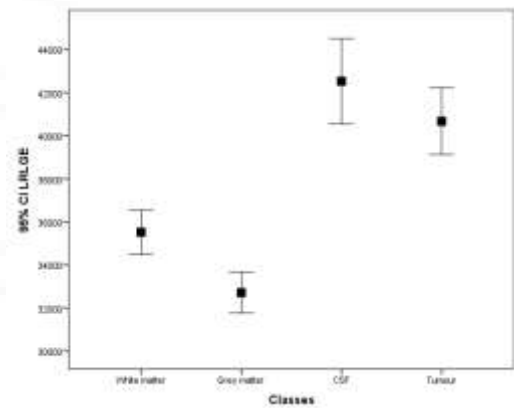


Figure 4.2.9: error bar shows the classification based on long run low gray-level emphasis feature

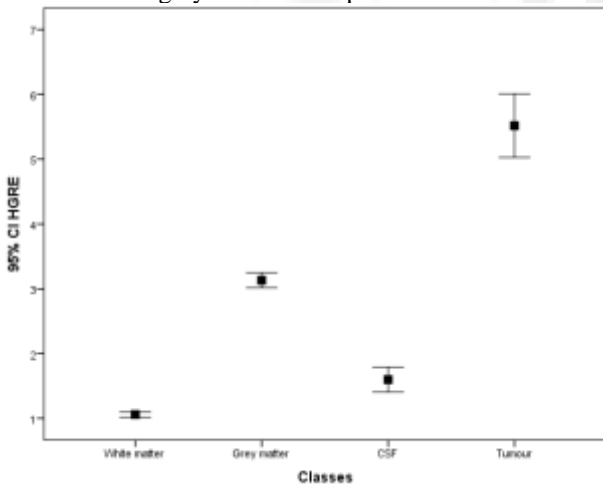


Figure 4.2.7: Error bar shows the classification based on high gray-level run emphasis feature

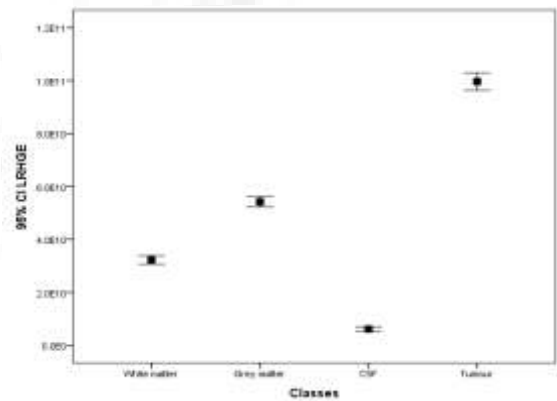
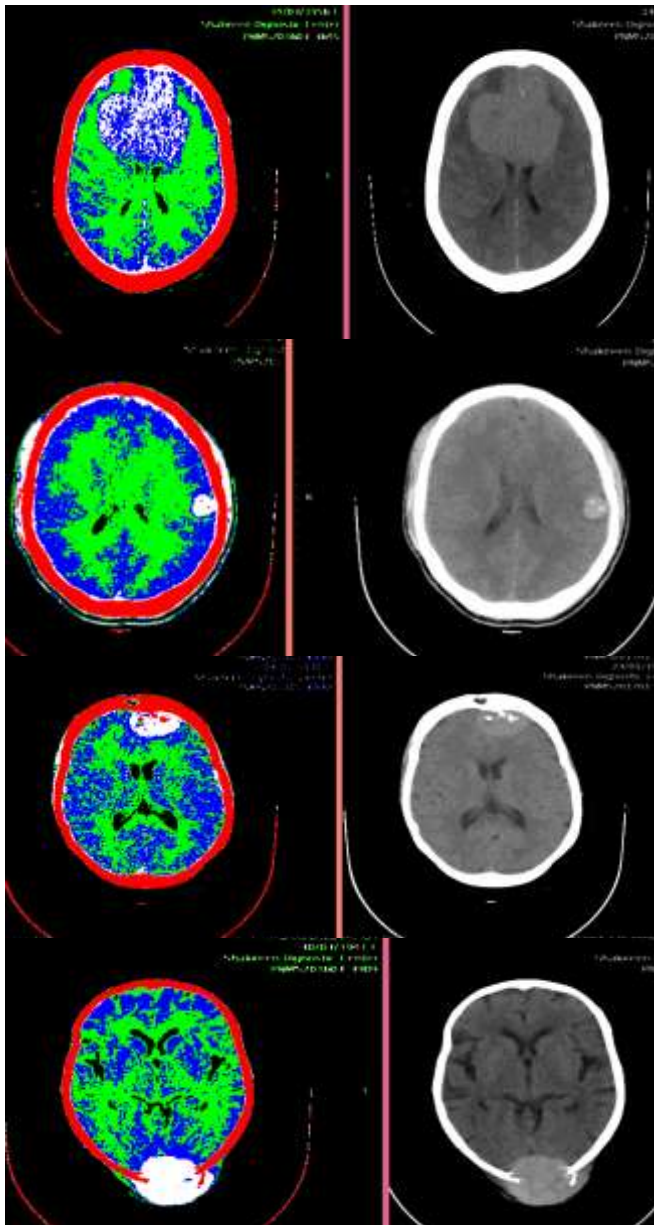


Figure 4.2.10: Error bar shows the classification based on long run high gray-level emphasis feature

The following images represent the classification intensity of the tumor and normal tissues.



5. Discussion

This is a retrospective study aimed to classify brain tumors in CT images using texture analysis.

One hundred and nine patients with different types of intracranial tumors were scanned using CT with similar protocol (5mm slice thickness, 5mm slice gap, pitch of one and 300mm FOV).

The images were diagnosed and classified by a well experienced MD radiologist into tumor, and normal intracranial component including white matter, gray matter and CSF using texture feature as input values.

The methodology consists of two order statistical analyses; **First order:** on which four features were selected (mean, skewness, energy and entropy) for the selected images. The quantitative data were analyzed using SPSS showing the following that the distances between the classified groups were large while it small between the classes within each

group this exploring the ability of system in well recognizing and differentiation of the classified groups Fig (4-1-1).

Table (4-1-1) demonstrate groups classification accuracy from which we can figure out there is a little interference between the tumor and white matter, 17% of tumor classes recognized as white matter this may due to existence of normal neuronal cells within the neoplasm. There is no tumor class recognized as gray matter or CSF.

To classify the tumor using the first order the result came out in respect to the extracted feature as; the mean significant discriminating feature that could be used to classify the brain tumor this explained on figure (4-1-2). While the accuracy was not high when the textural analysis based on the skewness as a discriminating feature as shown on figure (4-1-3) which demonstrate slightly poor differentiation between the tumor tissues and grey matter, and also failed to distinguish the white matter clearly separated from the CSF. When the classification based on the energy feature the method showed accurate differentiation between the neoplastic tissues and grey matter, CSF but there were some interference had been notice between the tumors and white matter when the classification based on the energy feature figure (4-1-4).

Figure (4-1-5) which demonstrate the classification based on the entropy it is obviously could be notice that the classification was accurate when it based on this feature, as it seen all the selected tissues had been represented as a separate group.

Higher order statistical analysis:

Fig (4-2-1) scatter graph represent the ability of the method differentiate between the interested tissues, this approved clearly on table (4-2-1) which demonstrate that the sensitivity, specificity and accuracy was 85.7%, 97%, 94.7 respectively

On this method nine features had been used including, long run emphasis, low gray-level run emphasis, high gray-level, Run emphasis, short run low gray-level emphasis, short run high gray-level emphasis, long run low gray-level emphasis, long run high gray-level emphasis, gray-level non-uniformity, run length non-uniformity, run percentage. The analyzed data showed results discussed as the following

Figures (4-2-2) to (4-2-10) error bars demonstrate the efficiency of the method on classifying the interested tissues in respect to the higher order features. The results shown up as the following:

Long run emphasis (LRE) feature classification based is not advisable method due to its limitation on recognizing the tumors as a different character from the CSF beside it also showed ill differentiation between grey and white matter figure (4-2-2).

Regard to grey level non uniformity (GLN) feature the system was very accurate to classify the white matter, grey matter and CSF and it has a considerable ability to separate

between them but a little bit interference were noticed between the tumor and grey matter fig (4-2-3) .

When it based upon the run length non uniformity feature (RLN) the system showed a deficiency on separating the grey matter from white matter, and tumor from CSF, but it clearly shown that the system successfully differentiates the neoplasm from grey-white matter fig (4-2-4). Same result came out when classification based on run percentage feature, in other words the system represented the grey and white matter as nearby characters, but differ from tumor and CSF which had also characterized have semi symmetrical textures figure (4-2-5).

Figure (4-2-6) which demonstrate the classification depend on low gray-level run emphasis feature, it clearly could be figured out that it is the most discriminating feature that can be used to characterize the SCF, but unfortunately the three of grey matter, white matter and tumor could never be classified using this feature because it represented as symmetrical characters of textural feature.

In respect to high gray-level run emphasis as classification feature the system Present ability to demonstrate the tumor and grey matter as different characteristic tissue component but ill differentiation between the white matter and CSF had been observed figure (4-2-7). Same results were achieved when classification based on short run high gray-level emphasis feature figure (4-2-8).

Like run percentage classification feature when the classification based on long run high gray-level emphasis feature the system represent the white-grey matter as nearby group and tumor-CSF as nearby group but each group demonstrated separate from the other one figure (4-2-9).

Figure (4-2-10) which demonstrate the classification based on long run high gray-level emphasis feature it showed same results to the classification when it based upon short run high gray-level emphasis feature showing well reorganization of the tumor from all selected tissues with considerable ability to recognize the normal tissue too.

The sensitivity of this method in recognizing tumor was 82.6%, specificity 98.1% and the accuracy was 90.4% this shows higher performance methodology compared to kimia rezaei and hamed agahi study

6. Conclusion

Sometimes it's very difficult to recognize the intracranial tumors from a non contrast CT image because the limitation of human eyes in differentiation the nearby values of gray scale. By using special software such as that has been used in this study, high diagnosis accuracy will be achieved.

By testing both of first order statistical analysis and the higher order we conclude that the higher order statistical analysis gives good result and much more accurate classification compared to the first order.

According to the results of first order statistical analysis the following formulas can be used to figure out to which tissue the numerical data belong to.

$$\text{Tumor} = (10.207\text{dA}) + (0.046\text{B}) + (4.949\text{C}) + (0.065\text{E}) - (1.15\text{F}) - 130.647$$

$$\text{White matter} = (10.722 \times \text{A}) + (0.025\text{B}) + (3.213\text{C}) + (0.088\text{E}) - (1.293\text{F}) - 104.880$$

$$\text{Gray matter} = (10.918\text{A}) + (0.028\text{B}) + (3.091\text{C}) + (0.068\text{E}) - (1.291\text{F}) - 121.020$$

$$\text{CSF} = (7.465\text{A}) + (0.026\text{B}) + (1.545\text{C}) + (0.093\text{E}) - (0.920\text{F}) - 50.799$$

While the following formulas had been established according to the higher order statistical analysis:

$$\text{White matter} = (\text{LRE} \times -0.001) + (\text{GLN} \times 1076.2) + (\text{RLN} \times 1.3) + (\text{RP} \times 0.063) + (\text{LGRE} \times 9404.4) + (\text{HGRE} \times -2.461) + (\text{SRHGE} \times -0.005) + (\text{LRLGE} \times 9.228^{-5}) + (\text{LRHGE} \times -1.6^{-10}) - 40.66$$

$$\text{Grey matter} = (\text{LRE} \times -0.001) + (\text{GLN} \times 1488.1) + (\text{RLN} \times 1.52) + (\text{RP} \times 0.061) + (\text{LGRE} \times 10353.92) + (\text{HGRE} \times -2.972) + (\text{SRHGE} \times -0.01) + (\text{LRHGE} \times -9.86^{-11}) - 51.183$$

$$\text{CSF} = (\text{LRE} \times -0.001) + (\text{GLN} \times 931.922) + (\text{RLN} \times 1.482) + (\text{RP} \times .086) + (\text{LGRE} \times 21758.651) + (\text{HGRE} \times -2.084) + (\text{SRHGE} \times -.004) + (\text{LRLGE} \times -2.231^{-05}) + (\text{LRHGE} \times -3.199^{-10}) - 57.183$$

$$\text{Tumour} = (\text{LRE} \times -0.001) + (\text{GLN} \times 1369.273) + (\text{RLN} \times 1.334) + (\text{RP} \times .066) + (\text{LGRE} \times 11052.766) + (\text{HGRE} \times -3.186) + (\text{SRHGE} \times -.004) + (\text{LRHGE} \times -5.226^{-11}) - 63.706$$

References

- [1] Brat, D. J, et al. Surgical neuropathology update: a review of changes introduced by the WHO classification of tumours of the central nervous system, 4th edition. Arch Pathol Lab Med, (2008). , 993-1007. Histology of Primary Brain Tumors <http://dx.doi.org/10.5772/52356> 175
- [2] Grisold, W, Oberndorfer, S, & Hitzzenberger, P. Editorial: Brain tumour treatment: the concept of inter- and multidisciplinary treatment. Wien Med Wochenschr, (2006). , 329-331
- [3] Hassoun, J, et al. Central neurocytoma: a synopsis of clinical and histological features. Brain Pathol, (1993). , 297-306
- [4] Koeller, K. K, & Rushing, E. J. From the archives of the AFIP: pilocytic astrocytoma: radiologic- pathologic correlation. Radiographics, (2004). , 1693-1708
- [5] Kovalev, V.; Gertz, H. & von Cramon D. (2001). Three-dimensional texture analysis of MRI brain datasets. IEEE Transactions on Medical Imaging, Vol. 20, No. 5, pp. 424-433.
- [6] Louis, D. N, et al. The 2007 WHO classification of tumours of the central nervous system. Acta Neuropathol, (2007). , 97-109
- [7] Marjolein van der Glas, 2000 Principles of Computerized Tomographic Imaging Mikael Sandborg, 1995, Computed Tomography: Physical principles and biohazards

- [8] Miller, C. R. & Perry, A. Glioblastoma. Arch Pathol Lab Med, (2007). , 397-406
- [9] Mirmehdi, M.; Xie, X. & Suri, J. (eds) (2008). Handbook of texture analysis, Imperial College Press, 1-84816-115-8, UK.
- [10] Pietikainen, M.K. (ed) (2000). Texture analysis in machine vision, World Scientific Publishing, 981-02-4373-1, Singapore.
- [11] Pradip R. Patel 2010, Lecture Notes Radiology, 3rd edition Published by Wiley-Blackwell. West Sussex PO19 8SQ, UK
- [12] Proceedings of 4th IASTED International Conference on Visualization, Imaging and Image Processing – VIIP, Marbella, Spain, September 6th – 8th.
- [13] Rorke, L. B. Pathologic diagnosis as the gold standard. Cancer, (1997). , 665-667.)
- [14] Sutton, R. and E. L. Hall, “Texture Measures for Automatic Classification of Pulmonary Disease,” IEEE Transactions on Computers, **C-21**, pp. 667-676, 1972.)
- [15] Tuceryan, M. & Jain, A.K. (1998). Texture analysis. In: Chen, C.H; Pau, L.F. & Wang, P.S.P., (eds). The handbook of pattern recognition and computer vision. 2nd ed. World Scientific Publishing Co., ISBN 9-810-23071-0, Singapore
- [16] Valerie C. Scanlon (2007) Essentials of Anatomy and Physiology. Fifth Edition – Philadelphia: F.A.Davis Company
- [17] Xu, D.; Kurani, A. & Raicu, D. (2004). Run-length encoding for volumetric texture,
- [18] Xu, Y.; Sonka, G.; McLennan, G.; Junfeng, G. & Hoffman, E. (2006). MDCT-based 3D texture classification of emphysema and early smoking related pathologies. IEEE Transactions on Medical Imaging, Vol. 25, No. 4, pp. 464-475.
- [19] Yu, H.; Caldwell, C.; Mah, K. & Mozeg D. (2009). Co-registered FDG PET/CT based textural characterization of head and neck cancer in radiation treatment planning. IEEE Transactions on Medical Imaging, Vol. 28, No. 3, pp. 374-383.

Author Profile



Auis bashir received the BSc. and MSc. degrees in medical diagnostic radiological science from Sudan University of science and technology in 2011 and 2015, respectively. During 2011-2018 he worked in several Sudanese hospitals as radiologic technologist dealing with different radiologic modalities and machines that used on the medical field beside he held many positions during these period, like clinical instructor, lecturer, academic research supervisor and headmaster of clinic x.ray department.



Mr. Shazaly Nader Khojaly Mansour (Sudan) received (B.Sc.) in diagnostic radiology technology and (M.Sc.) in medical ultrasound imaging from College of Medical radiological Science, Sudan University of Science and Technology in 2011 and 2015 respectively. Now as Sonographer in Hamad Medical Corporation, Doha ,Qatar from 2018 up to now